Renewable rarasaponin-bentonite-alginate composite with sponge-like structure and its application for crystal violet removal from aqueous solution

Livy Laysandra[a], Rizka Fabryanty[a], Yi-Hsu Ju[b], Jindrayani Nyoo Putro[c], Shella Permatasari Santoso[a], Felycia Edi Soetaredjo[a,*], Alfin Kurniawan[c], Suryadi Ismadji[a,*]

[a]*Department of Chemical Engineering, Widya Mandala Surabaya Catholic University, Kalijudan 37, Surabaya 60114, Indonesia, Tel. +6231 389 3933, Fax +6231 389 1267, email: livy.laysandra@yahoo.com (L. Laysandra), rizka.fabryanty12@gmail.com (R. Fabryanty), shella_p5@yahoo.com (S.P. Santoso), felyciae@yahoo.com (F.E. Soetarejo), suryadiismadji@yahoo.com (S. Ismadji)*
[b]*Graduate Institute of Applied Science and Technology, National Taiwan University of Science and Technology, No. 43, Sec 4, Keelung Rd, Da'an District, Taipei City 106, Taiwan, Tel. +886 2 2730 3609, email: yhju@mail.ntust.edu.tw (Y.-H. Ju)*
[c]*Department of Chemical Engineering, National Taiwan University of Science and Technology, No. 43, Sec 4, Keelung Rd, Da'an District, Taipei 106, Taiwan, Tel. +886 2 2737 6611, Fax +886 2 2737 6644, email: jindranyoo@yahoo.com (J.N. Putro), alfin_kur@yahoo.com (A. Kurniawan)*

Received 6 October 2018; Accepted 31 March 2019

ABSTRACT

Adsorption is an efficient process for removing contaminants from water by using adsorbent. In this work, bentonite, rarasaponin, and sodium alginate are used as raw materials to prepare new composite to be applied to the adsorption of crystal violet dye. The prepared adsorbent (bentonite-rarasaponin-alginate composite) has a sponge-like appearance. The Fourier transform infrared (FTIR), X-ray diffraction (XRD), nitrogen (N_2) sorption and scanning electron microscopy (SEM) methods were employed to characterize the prepared adsorbents. The adsorption experiments were conducted isothermally at 30,50, and 70°C. The Freundlich and Langmuir isotherm models were chosen to correlate the equilibrium adsorption data. Meanwhile, the adsorption kinetics was studied at 30°C, and the data were correlated by using the pseudo-first-order and pseudo-second-order. Based on the adsorption results, it was found that composite can adsorb crystal violet dye 3 times more than bentonite at all investigated temperatures, where at 70°C the adsorption capacity for acid-activated bentonite is 176.63 mg/g and for rarasaponin-bentonite-alginate composite is 476.04 mg/g. The adsorption of crystal violet dye onto the adsorbents increases with increasing temperature indicating that the chemisorption is dominant in this process.

Keywords: Acid activated bentonite; Rarasaponin; Sodium alginate; Composite; Isotherms; Kinetics

1. Introduction

Contamination of surface water by synthetic dyes is a serious environmental problem. Most of these contaminants come from the effluent of textile industries. Some of the synthetic dyes are found to be resistant to microbial degradation, causing their presence in water environment harmful to aquatic organisms. Some techniques can be employed to remove the synthetic dyes from water, some

of them are biological treatment, coagulation, floatation, oxidation, ozonation, nanofiltration, and adsorption [1–3]. Among the techniques available, adsorption is used more often because this technique is inexpensive, environmentally friendly, and more importantly effective against most types of contaminants [4]. The success of the adsorption process which is indicated by the high removal of contaminant is strongly influenced by the type adsorbent. Activated carbon is a commercial adsorbent with good surface reactivity which is often used especially for the separation and purification of water from organic compounds such as syn-

*Corresponding author.

thetic dyes. However, the commercially available activated carbons are expensive; therefore the use of activated carbon for water and wastewater treatment is economically unfeasible. To overcome this, the developments of alternatively low-cost adsorbents which are inexpensive, harmless, and have high adsorption capacity are needed [5–7].

Bentonite mainly consists of smectite montmorillonite, bentonite also commonly called as montmorillonite. The natural and chemically modified bentonites are well known as alternative cheap adsorbents, they have large Brunauer-Emmett-Teller (BET) surface area due to its layered structure. The adsorption affinity of bentonite can be increased by modifying it with an intercalating agent (i.e., surfactant). The affinity enhancement enables bentonite to be employed for a wider variety of pollutants [8]. In order to avoid environmental problems that might arise from the use of synthetic surfactants, the use of an environmentally friendly (natural) surfactant is more desirable [9]. Some studies related to adsorption properties of intercalated bentonite have been reported. A study by Kurniawan et al. reported that bentonite intercalated with the extract from *SapindusrarakDC* (rarasaponin) can adsorb 256 mg Methylene Blue per g adsorbent (at 60°C), while raw bentonite can only adsorb 194 mg methylene blue per g adsorbent (at 60°C) [9]. Fosso-Kankeu et al. reported that bentonite intercalated by cationic surfactant hexadecyltrimethyl ammonium bromide can adsorb 16.04 mg Congo Red per g of adsorbent, while the natural bentonite can adsorb 5.00 mg Congo Red per g of adsorbent [10]; Özcan et al. reported that bentonite intercalated with cationic surfactant dodecyltrimethyl ammonium bromide can adsorb 206.58 mg Reactive Blue 19 per g adsorbent [11]. Study on the intercalation of cetyltrimethyl ammonium bromide (CTAB) into another type of clay mineral, namely kaolin, by Zenasni et al., also showed that CTAB-kaolin can adsorb 24.46 mg Congo Red per g adsorbent which is 4 times higher than natural kaolin (5.94 mg Congo Red per g adsorbent) [12]. In this work, rarasaponin is used as a surfactant for intercalation. Intercalation process can increase the number of active sites, surface area and interlayer spacing of natural bentonite. The intercalation of rarasaponin molecules into the interlayer of bentonite occurs in several stages; the first stage is deacylation of rarasaponin due to the dissolution in the polar solvent, this causes rarasaponin to be negatively charged; the second stage is protonation of the silanol group on bentonite so that the bentonite is positively charged; and the last stage is charge balancing through the interaction between the two differently charged molecules [13].

In this work, a natural polymer, sodium alginate, is combined with rarasaponin-bentonite in order to further increase the adsorption capacity. The main purpose of this work is to prepare a new, low-cost, and environmentally friendly adsorbent composite with high adsorption capacity for the removal of organic dye from aqueous solution. Some analyses including FTIR, XRD, SEM,and nitrogen sorption were employed prior to characterizing the prepared rarasaponin-bentonite-alginate composites. The formation mechanism of the composite is also given in this manuscript. The adsorption ability of the composites was investigated against a cationic dye, Crystal Violet. The adsorption was conducted isothermally and kinetically.

2. Materials and methods

2.1. Materials

The bentonite used in this study is natural calcium-exchanged bentonite (Ca-bentonite) obtained from the mining site at Pacitan, East Java, Indonesia. *Sapindusrarak DC* was obtained from Klaten, Central Java, Indonesia. The natural surfactant, rarasaponin, was obtained by extracting the fruit pericarp of *Sapindusrarak DC*. The detailed procedure of rarasaponin extraction can be seen elsewhere [9]. Sodium alginate was supplied from CV. Nura Jaya, Surabaya, Indonesia. Analytical grade crystal violet (purity > 90%, $C_{25}H_{30}Cl$, M_w 407.98 g/mol) was purchased from Sigma Aldrich, Singapore. The chemicals are used as received without further purification.

2.2. Preparation of rarasaponin-bentonite and rarasaponin-bentonite-alginate composite

Ca-bentonite was acid-activated by mixing with 5 N H_2SO_4 solution (1:10 w/v ratio) under constant stirring at 500 rpm and 70°C for 2 h. The acid-activated bentonite was rinsed with distilled water until the pH of the rinse water was constant. Subsequently, the acid-activated bentonite was dried at 105°C in an oven (Memmert UM 400) for 24 h. The dried acid-activated bentonite was pulverized into powder and sieved using vibration screener (Retsch AS 200) to obtain a particle size of –180/+200 mesh.

The rarasaponin-bentonite was synthesized according to the procedure reported by Kurniawan et al. (2012) [14], briefly1 g of rarasaponin was dissolved into 50 mL distilled water, then10 g of acid-activated bentonite was added to the solution. Rarasaponin was dissolved in advance with the aim of increasing the contact surface area between rarasaponin and acid-activated bentonite. After mixing, the mixture was irradiated in a microwave oven at 700 W (National NN-S327 WF) for 3 min.

The rarasaponin-bentonite-alginate composite was prepared according to the same procedure [14] as rarasaponin-bentonite with slight modification; briefly 0.45 g of rarasaponin was mixed with 25 mL distilled water. The rarasaponin solution was vigorously stirred until the rarasaponin solution is foamy. Subsequently,acid-activated bentonite was added to the rarasaponin solution with a mass ratio of acid-activated bentonite to rarasaponin of 10:1. The mixture was stirred at 500 rpm for 10 min, and then 0.5 g of sodium alginate was added to the mixture. The mixture of sodium alginate, acid activated bentonite, and rarasaponin was then heated at 70°C under constant stirring at 800 rpm for 1 h. After the heating, mixture slurry was obtained and then slowly transferred into 200 mL of 0.3 N $CaCl_2$ solution to form granules rarasaponin-bentonite-alginate composite. The excess $CaCl_2$ on the surface of the composite was repeatedly washed using reverse osmosis water and dried in an oven at 50°C for 12 h.

2.3. Characterization of the samples

The characterization of the samples, namely acid-activated bentonite, rarasaponin-bentonite, and rarasaponin-bentonite-alginate composite,was conducted by using

Fourier-transform infrared spectroscopy (FTIR), X-ray diffraction (XRD), SEM (scanning electron microscopy), and nitrogen sorption methods.

The FTIR analysis was carried out using FTIR SHIMADZU 8400S, KBr pellet method was employed to obtain the spectra of the samples. The spectra were scanned at a wavelength range of 4000 400 cm^{-1} with a resolution of 2 cm^{-1}.

The XRD analysis was conducted by using a Philips X'pert X-ray Diffractometer. The XRD patterns were acquired at 40 kV and 30 mA with Cu Kα_1 (l = 0.15405 nm) as the source of radiation.

The surface topography was obtained by using a JEOL JSM-6500 F field emission SEM at 10 kV and WD 10.1 to 10.3 mm. Prior for SEM, the samples were coated with thin layer (3 nm) of platinum/palladium (Pt/Pd) alloy using an auto fine coater JEC-3000 F. The coating process was carried out in Argon atmosphere for 90 s.

The BET surface area was determined by using automatic sorption analyzer Micromeritics ASAP 2010. The measurements were conducted at –195.8°C (boiling point of nitrogen) over a relative pressure of 0.001–0.995. The samples were degassed at 150°C under high vacuum before each measurement. The BET surface area was calculated at a relative pressure in the range of 0.05–0.35.

The point of zero charge (pH$_{pzc}$) of each adsorbent used in this study was determined by using the pH drift method [15], and it was found that pH$_{pzc}$ of acid-activated bentonite is 3.08, rarasaponin-bentonite is 3.44, and the rarasaponin-bentonite-alginate composite is 4.08.

2.4. Adsorption of dye

The optimal pH for the adsorption of crystal violet onto the prepared adsorbents is studied in the pH range of 2–10, with initial crystal violet concentration of 800 ppm, a temperature of 30 ± 1°C, for 8 h. The pH was adjusted using 0.1 N of HCl or NaOH solutions. After equilibrium, the adsorbent was separated by using a centrifuge, and the concentration of un-adsorbed crystal violet in the filtrate was then analyzed using Shimadzu UV/Vis-1700 spectrophotometer at a wavelength of 590 nm.

The adsorption equilibrium experiments were performed in batch. A stock solution of 800 ppm crystal violet dye at a certain pH was prepared by dissolving a certain amount of crystal violet in 1000 mL distilled water. Subsequently, the crystal violet solution was distributed in a series of Erlenmeyer flasks (50 mL of solution in each flask). A various mass of adsorbent was then introduced to the series of Erlenmeyer flasks. The adsorption was conducted for 8 h in a Memmert shaking water bath at various temperatures of 30, 50, 70 ± 1°C. After adsorption, the solution was centrifuged at 4700 rpm for 5 min to separate the solution from solid adsorbent particles. The concentration of crystal violet in the solution before and after the adsorption process was measured using a Shimadzu UV/Vis-1700 spectrophotometer at maximum absorbance wavelengths of 590 nm. All adsorption experiments were repeated at least three times to ensure the accuracy of the obtained data. The dye removal efficiency was calculated in percentage by using Eq. (1), while the amount of crystal violet adsorbed at equilibrium condition was calculated by using Eq. (2).

$$\% \text{ dye removal} = \frac{(C_i - C_e) \times 100}{C_i} \tag{1}$$

$$q_e = \frac{(C_i - C_e) \times V}{m} \tag{2}$$

where q_e is the amount of dye adsorbed at equilibrium (mg/g adsorbent), C_i and C_e (mg/L) are the initial and equilibrium crystal violet dye concentration, respectively, V (L) is the volume of the dye solution, and m (g) is the mass of the adsorbent.

For the kinetic adsorption experiments, 0.5 g of the adsorbent was introduced into a series of 50 mL crystal violet solution with various initial concentrations (600, 800, and 1000 ppm). The adsorption was performed in a shaker water bath (200 rpm), and a temperature of 30°C. The kinetic adsorption data were collected by taking one of the samples at a certain period of time. The solid adsorbent was then separated from the filtrate by using centrifugation technique. The concentration of remaining crystal violet dye in the filtrate was measured quantitatively by using a spectrophotometer. The amount of crystal violet adsorbed onto adsorbent at a certain time (t) was calculated using Eq. (3).

$$q_t = \frac{(C_i - C_t) \times V}{m} \tag{3}$$

where C_t is the crystal violet concentration in the solution at time t.

2.5. Goodness of fitting analysis

The goodness of fitting between experimental data and calculated data for each non-linear adsorption models is measured by determining the coefficient of determination (R^2), hybrid fractional error function (HYBRID), and Marquardt's percent standard deviation (MPSD) [16,17]. The R^2 shows the measurement of how close the fitting of experimental data is to the calculated data, this coefficient has a degree in the range of 0–1. The HYBRID error function is an improvement to that of classic error function namely sum of squared errors (SSE), the improvement is especially at to minimize the magnitude of the errors at a lower level of liquid-phase concentration. The MPSD is an error function that shows the geometric mean error based on the number of degree of freedom in the investigated system [16–19].

3. Result and discussion

For the purpose of simplification, acid-activated bentonite, rarasaponin-bentonite, and rarasaponin-bentonite-alginate are abbreviated as AAB, RB, and RBA, respectively.

3.1. Characterization of the adsorbents

The FTIR spectra of AAB, RB, and RBA composite are shown in Fig. 1. Both RB and RBA composite possesses spectra originated from rarasaponin and bentonite. There are some slight shifts observed for the spectra of RBA composite compared with RB. The broad band corresponds to
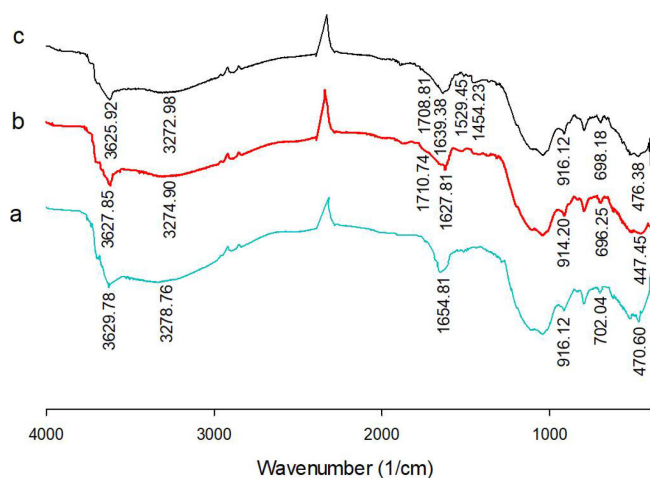
Fig. 1. FTIR spectra of (a) AAB, (b) RB, and (c) RBA composite.

the stretching of the –OH (hydroxyl) groups are found at the wavenumber of 3629.78, 3627.85 and 3625.92 cm^{-1} for AAB, RB, and RBA composite, respectively. Bands at 3278.76 (AAB), 3274.90 (RB),and 3272.98 (RBA composite) cm^{-1} responsible for the vibration of –OH strectching which represents the bond between –OH group and Al or Si. The presence of rarasaponin is indicated by the appearance of the band at 1710.74 and 1708.81 cm^{-1} for RB and RBA composite, respectively, where the bands are attributed to the stretching vibration of C=O bonds; these bands also indicate ions exchange between Ca^{+2} from bentonite against the acetyl cation (C$_2$H$_3$O$^+$) from rarasaponin [9]. The –OH bending of H$_2$O at interlayer of bentonite is indicated by the peaks at 1654.81cm^{-1} for AAB, 1627.81 cm^{-1} for RB and 1639.38 cm^{-1} for RBA composite. The Al–Al–OH bending vibration was observed at 916.12 (AAB), 914.20 (RB), and 916.12 cm^{-1} (RBA composite); Al–O–Si bending vibration was observed at 702.04 (AAB), 696.25 (RB), and 698.18 cm^{-1} (RBA composite); and Si–O–Si bending vibration was observed at 470.60 (AAB), 447.45 (RB), and 476.38 cm^{-1} (RBA composite).

Alginate compound was added for the preparation of the RBA composite. The interaction of alginate with rarasaponin/bentonite was indicated from the appearance of new bands at 1529.45 and 1454.23 cm^{-1}, where these bands correspond to the asymmetrical and symmetrical stretching vibrations of the carboxylic groups (–COO$^-$). The bands also indicate that the alginate molecules have successfully binded to the silanol group by releasing cationic Na$^+$ from sodium alginate compound. For easy reference, the wavenumber values and their corresponding surface functional groups are tabulated in Table 1.

The X-ray diffraction (XRD) spectra of the solid adsorbents are given in Fig. 2. The intercalation of rarasaponin to the interlayer of bentonite leads to the shift of basal spacing of bentonite. Originally, the AAB has a *d* spacing (001) of 1.36 nm. The intercalation of rarasaponin causes the *d* spacing to increase to 1.54 nm and 1.58 nm for RB and RBA composite, respectively. Some characteristic peaks of quartz are also observed in Fig. 2.

The surface topographies of the adsorbents were observed by using SEM and the images are depicted in Fig. 3. Different surface morphologies are observed for AAB,

Table 1
Surface functional groups of the AAB, RB, and RBA composite

| Functional group	Wave number (cm^{-1})		
	AAB	RB	RBA composite
-OH stretching in the hydroxyl group	3629.78	3627.85	3625.92
-OH stretch of (Al or Si) -OH group	3278.76	3274.90	3272.98
-OH bending of H$_2$O at interlayer bentonite for adsorbed	1654.81	1627.81	1639.38
Al-Al-OH bend	916.12	914.20	916.12
Al-O-Si bend	702.04	696.25	698.18
Si–O–Si bend	470.60	447.45	476.38
C=O stretch (C$_2$H$_3$O$^+$)	–	1710.74	1708.81
COO$^-$ asymmetrical stretching of alginate	–	–	1529.45
COO$^-$ symmetric stretching of alginate	–	–	1454.23
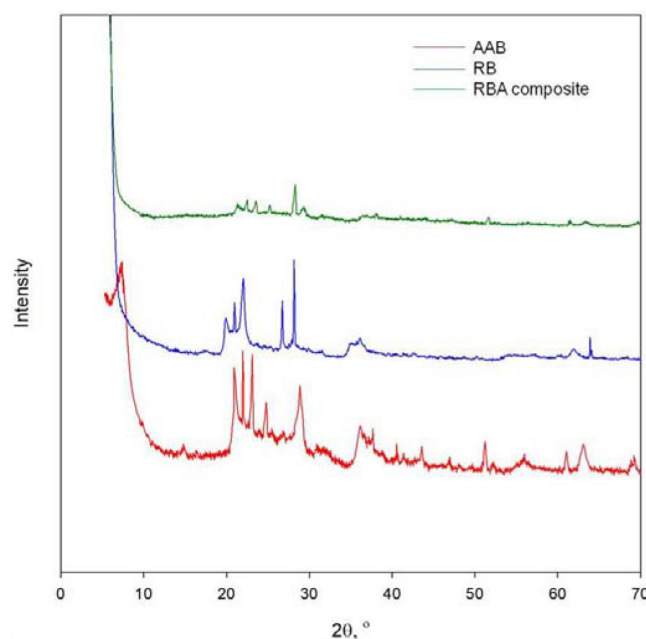
Fig. 2. X-ray diffraction spectra of (a) AAB, (b) RB, and (c) RBA composite.

RB, and RBA composite. The SEM images of RB (Fig. 3b) and RBA composite (Fig. 3c) show a larger particle size compared to AAB (Fig. 3a); this indicates that the addition of alginate, as well as rarasaponin, causes the bentonite particles to join and form larger particles. The addition of rarasaponin (in the formation of RB) only produced a weak interaction between the rarasaponin and bentonite thus the RB still have a powder form (bigger than AAB). In the formation of RBA composite, the addition of alginate causes the RB particles to join together with a stronger interaction to form larger particles which have a sponge-like structure (Fig. 3d).
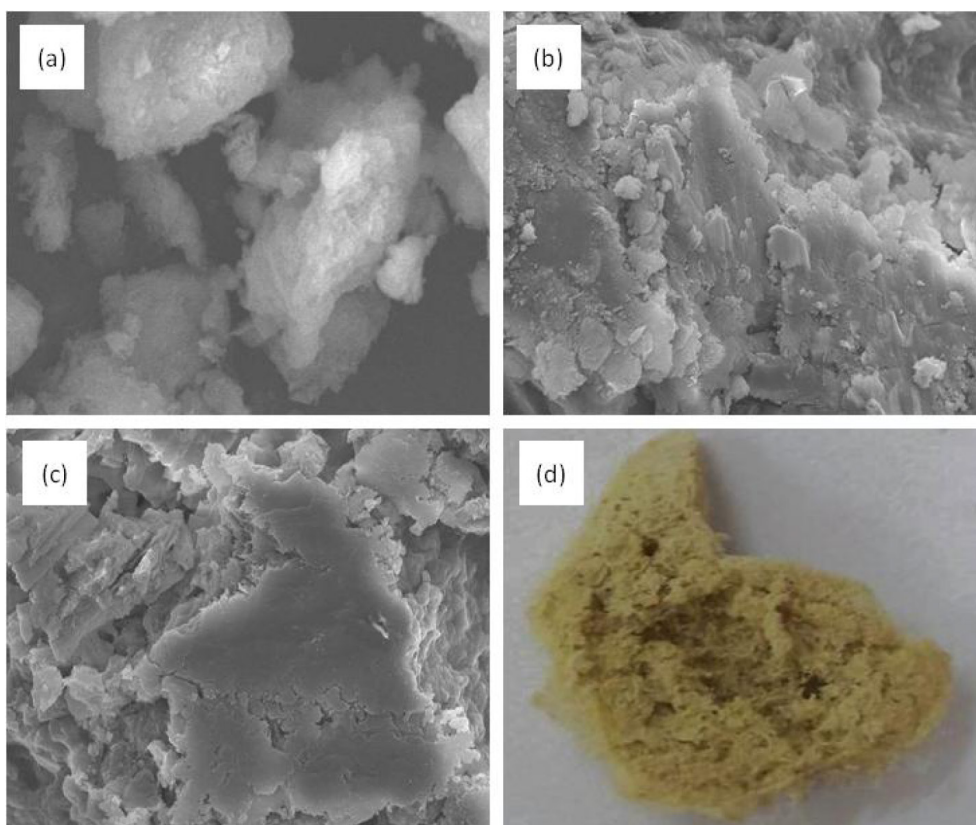
Fig. 3. SEM topography images of (a) AAB, (b) RB, and (c) RBA composite. Image (d) show the digital photograph of the RBA composite.

The nitrogen sorption isotherms of the AAB, RB, and RBA composite are given in Fig. 4. All of the adsorbents performed a rapid intake of nitrogen gas molecules at a low relative pressure (p/p^o). This phenomenon indicates that all of the adsorbents have a microporous structure (type I isotherm). Broad hysteresis loops at p/p^o above 0.4 suggest that the adsorbents also have a mesoporous structure (type II isotherm). RB and RBA possess broader hysteresis loop than AAB, where RB has the broadest loop. The broaden hysteresis loop indicates that the intercalation of rarasaponin into interlayer of bentonite created the more complex structure with some interconnected interlayer. The BET surface area for AAB, RB, and RBA composite is 73.7 m^2/g, 88.3 m^2/g, and 97.8 m^2/g, respectively. The pore volume of AAb, RB, and RBA composite is 0.121 cm^3/g, 0.376 cm^3/g, and 0.392 cm^3/g, respectively.

3.2. Effect of pH on the adsorption of crystal violet onto the adsorbents

The adsorption of crystal violet on the surface of the adsorbents is very dependent on the pH of the solution. The pH of the solution affects the surface charge of the adsorbents and also the regulation of ionization of the adsorbate. The point zero charge (pH$_{pzc}$) of the adsorbents are depicted in Fig. 5, where AAB, RB, and RBA composite have pH$_{pzc}$ of 3.20, 3.40, and 4.06, respectively. The adsorbent will have a positive surface charge when the pH of the solution below
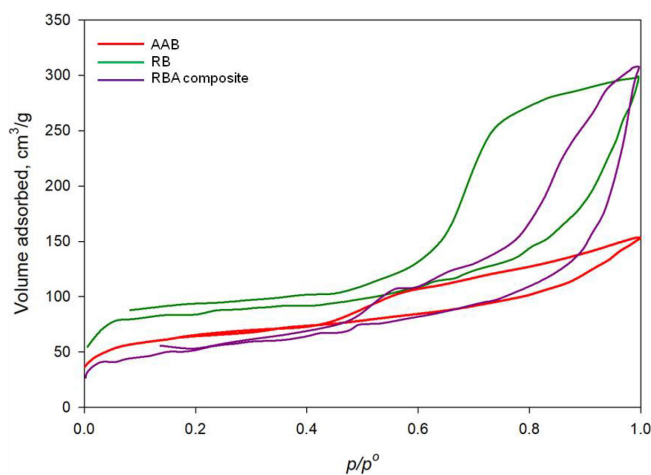

Fig. 4. Nitrogen sorption isotherms of AAB, RB, and RBA composite.

their pH$_{pzc}$, and have a negative surface charge at the pH above the pH$_{pzc}$.

The effect of pH on the adsorption of crystal violet onto AAB, RB, and RBA composite can be seen in Fig. 6. The adsorption capacity of the adsorbents increases at the pHs above their pH$_{pzc}$. At pH below pH$_{pzc}$, the interaction between cationic crystal violet dye and positively charged
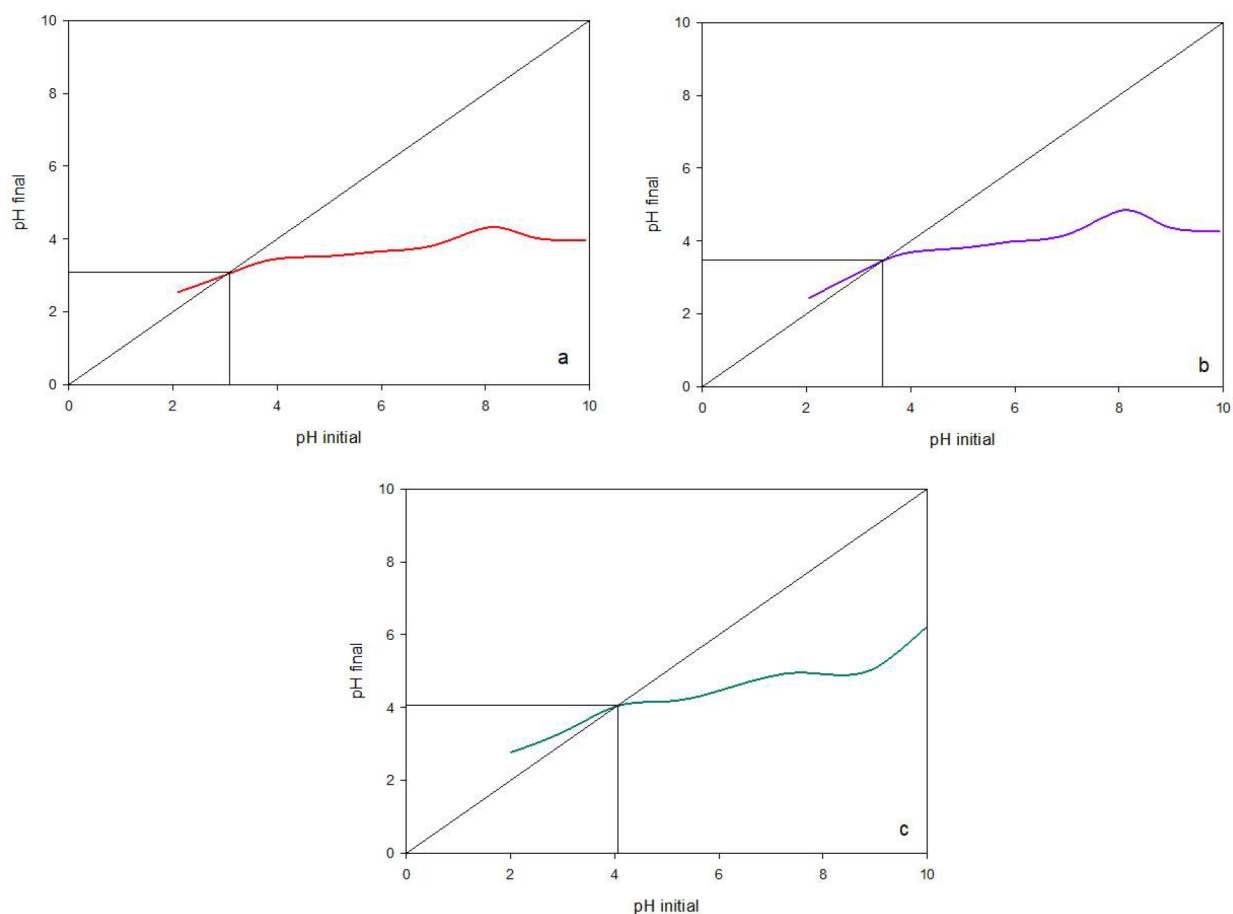
Fig. 5. The point of zero charges (pHpzc) of (a) AAB, (b) RB, and (c) RBA composite.
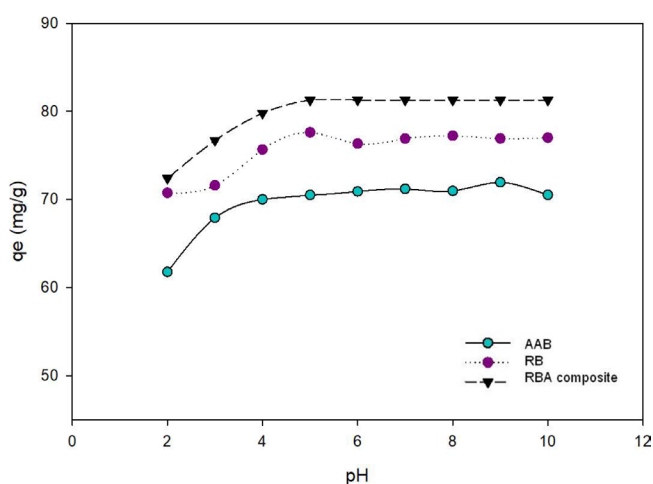

Fig. 6. Effect of pH on the adsorption of crystal violet onto AAB, RB, and RBA composite.

bentonite leading to repulsion of the dye from the surface of the adsorbents thus decrease the adsorption capacity. At pH above pH_{pzc}, the electrostatic attraction force between cationic crystal violet and negatively charged bentonite occurred thus leading to the higher amount of the dye attached onto the surface of the adsorbents. As the pH increases, the silanol group of bentonite became deprotonated thus increasing the number of negative sites on the surface of adsorbents [20]. The highest removal efficiency of crystal violet was found to be 90% for AAB, 96.32 % for RB, and 99.89% for RBA composite.

3.3. The formation mechanism of RBA composite

The formation mechanism of RB by intercalating bentonite with rarasaponin has been described by Kurniawan et al. 2011 [9]. The formation mechanism of the RBA composite by combining RB and sodium alginate is presented in this section. The schematic of the proposed formation mechanism is presented in Fig. 7. The formation mechanism of RBA composite occurred as follow: in the AAB molecules, the silanol group on the tetrahedral layer of AAB is protonated by the occurrence of H^+ion since the $pH_{solution}<$ pH_{pzc}, therefore the –OH of silanol group is protonated into $–H_2O^+$. In the rarasaponin molecules, dissolution of rarasaponin in the water cause the two acyl groups (at carbonyl structure) to be deacylated and produced sites with a negative charge. These negatively charged sites are the active binding sites against the positively charged bentonite. As for the natural polymer sodium alginate (Na-alginate), the Na^+ ion attached to the carboxyl structure will be released
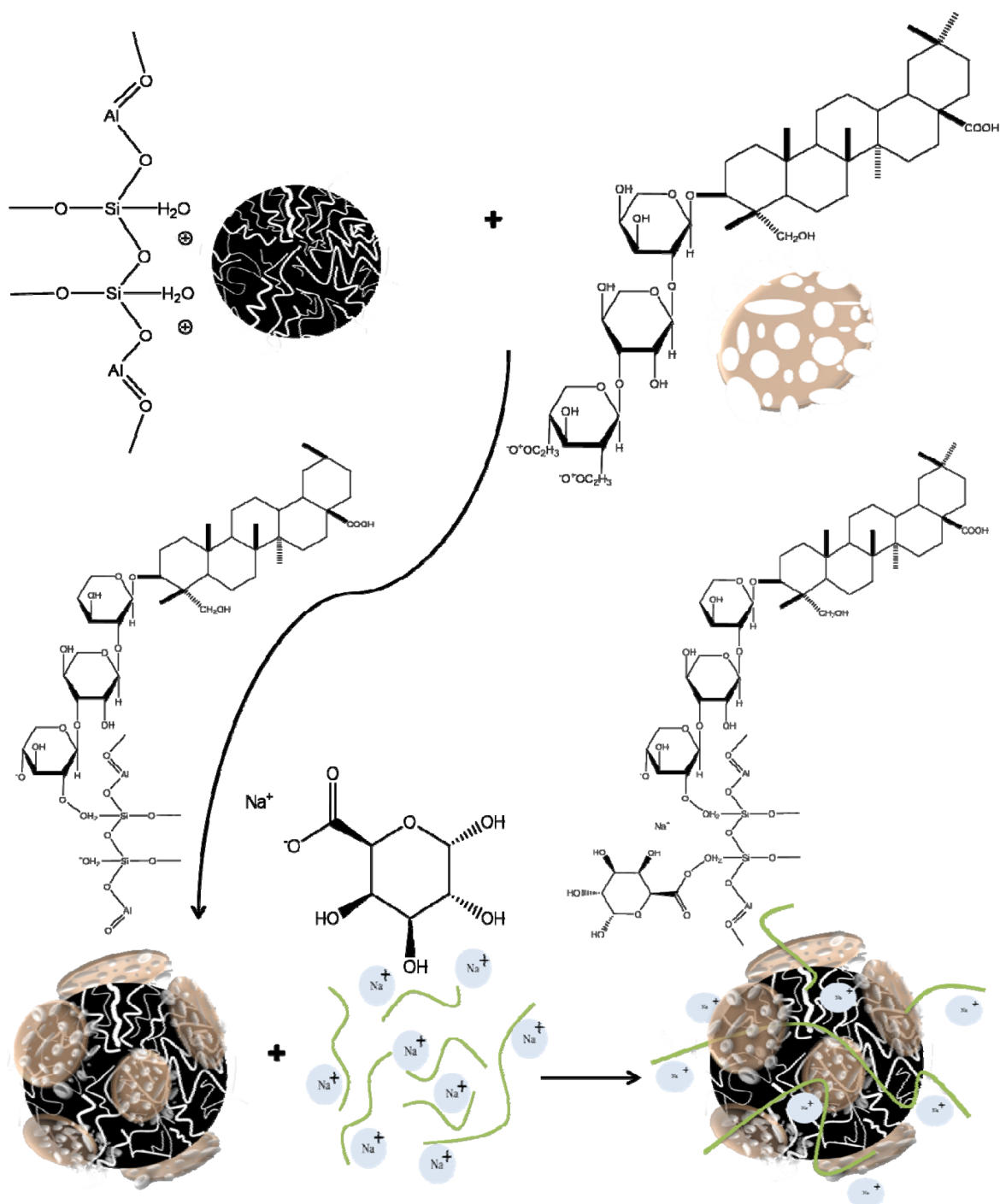
Fig. 7. The proposed formation mechanism of rarasaponin-bentonite-alginate (RBA) composite.

as it is dissolved in water and produced an anionic polymer with the negatively charged carboxyl group($-COO^-$) [21]. The $-COO^-$ group also contributes as an active binding site for positively charged bentonite. The addition of alginate also induced a gelation process; thus the rarasaponin/bentonite particles are attracted together. The final step, the rarasaponin/bentonite/alginate mixture is transferred into $CaCl_2$ solution. The Ca^{2+} ions from $CaCl_2$ are induced cross-linking between the alginate polymers and produced a rigid gel, where the cross linking occurs between the unbinding $-COO^-$ groups of the alginate with the pattern of $-COO^-$–Ca^{2+}–COO^- [22].

3.4. Equilibrium adsorption isotherm studies

The equilibrium adsorption isotherm models can describe how the adsorbate molecules distributed in the solution. The models also can be used to determine the parameters

in adsorption equilibrium [23,24]. Langmuir and Freundlich adsorption models were employed to investigate the adsorption equilibria data in a single system at three different temperature of 30, 50, and 70°C. The Langmuir model describes the mono layer adsorption on the homogeneous surface. The Langmuir equation is written as follows:

$$q_e = q_m \frac{K_L C_e}{1 + K_L C_e} \qquad (4)$$

where q_m is the Langmuir constant, which indicates the adsorption capacity of the adsorbent (mg/g), while K_L represents the adsorption affinity between adsorbate and adsorbent (L/mg).

Freundlich equation describes the adsorption behavior of the heterogeneous systems. The Freundlich equation has the following mathematical form:

$$q_t = \frac{k_s q_e^2 t}{\left(1 + \left(k_s q_e t\right)\right)} \qquad (5)$$

where K_F represents the adsorption affinity (mg/g)(mg/L)$^{-n}$ and n is a Freundlich constant which represents the heterogeneity of the system [18].

The fitted parameters of Langmuir and Freundlich models obtained from the fitting of the experimental data are summarized in Table 2, while the plots are given in Fig. 8. As shown in Fig. 8, the amount of adsorbed crystal violet dye molecules is increased along with the increase of temperature for all systems, indicating that chemisorption is the most dominant process in this adsorption. The increase of temperature helps to increase the adsorption affinity and cause the interaction between adsorbents and dye molecules becomes stronger; thus the adsorption capacity increases.

Both adsorption capacity (q_m) and adsorption affinity (K_L), the parameters in Langmuir model, are temperature dependence parameters. In an exothermic adsorption process, the increase in temperature gives a negative impact on these parameters. Meanwhile, in endothermic adsorption, the increase in temperature gives a positive impact on the parameters. As shown in Table 2, the value of q_m and K_L increase with the increase of temperature thus indicate an endothermic adsorption process.

Similar to Langmuir model, the parameters K_F and n in Freundlich model are also temperature dependence. For a physisorption process, the values of K_F and n will decrease as the temperature increases; while in chemisorption, the increase in temperature will give rise to the value of the parameters. In the adsorption of crystal violet onto the AAB, RB, and RBA composite, the parameter K_F and n increase as the adsorption temperature increases thus supported the chemisorptions process. With the increase of temperature, there is more heat energy available to be converted into kinetic energy and leading to greater interaction between crystal violet dye molecules and surface of adsorbents. Parameter n in Freundlich also represents the heterogeneity of the surface of adsorbent; as the temperature increases, the value of parameter n also increased, this is due to the increase of the system heterogeneity.

Based on the data and calculated parameters, both Langmuir and Freundlich models gave reasonable and consistent values of their parameters. In the AAB system, the data fitting by using Freundlich equation gave better values of R^2 than that of Langmuir model. The *HYBRID* and *MPSD* values also indicate that experimental and calculated data in Freundlich are closer to each other than in Langmuir. Therefore, from this point of view, the Freundlich equation represents the data better than Langmuir the AAB system.

Table 2
Langmuir and Freundlich parameters for the adsorption of crystal violet onto AAB, RB, and RBA composite

Adsorbent	T (°C)	Langmuir Parameters						Freundlich Parameters				
		q_m (mg/g)	K_L (L/mg)	R_L	$R^{2\dagger}$	HYBRID§	MPSD‡	K_F (mg/g) (mg/L)$^{-n}$	n	$R^{2\dagger}$	HYBRID§	MPSD‡
AAB	30	141.0932	0.1766	0.00703	0.8752	609.3664	90.3100	46.5350	5.1009	0.9929	25.5953	17.5692
	50	156.7306	0.2971	0.00419	0.8971	535.2573	81.6030	55.0873	5.1140	0.9820	78.2889	30.3660
	70	176.6300	0.4476	0.00278	0.8706	814.4050	104.4755	64.7932	5.1256	0.9815	145.1187	39.3272
RB	30	191.3284	0.7214	0.00173	0.9338	305.4419	44.6472	74.6830	5.4973	0.9560	408.5259	70.7110
	50	199.0631	0.7223	0.00173	0.9379	281.5130	43.3734	78.3167	5.5952	0.9406	563.4575	83.2349
	70	270.9195	0.7923	0.00158	0.9220	632.0558	83.2288	103.5830	5.6031	0.8421	1815.4867	155.0829
RBA composite	30	398.5130	0.2320	0.00536	0.9242	687.7220	67.6047	93.7641	3.4687	0.9481	1518.7219	139.3445
	50	454.2653	0.2334	0.00533	0.9523	511.6368	63.8123	104.8552	3.4823	0.9247	2225.9307	168.6787
	70	476.0389	0.2554	0.00487	0.9144	1206.8137	99.6014	113.0104	3.4847	0.8913	3072.5068	199.7183

†R^2 is sum squares of residuals between calculated and experimental data; the value was obtained directly from data fitting by using Sigma plot.

§HYBRID = $\dfrac{100}{n-p} \sum \dfrac{\left(q_{e,exp} - q_{e,cal}\right)^2}{q_{e,exp}}$

‡MPSD = $100 \sqrt{\dfrac{1}{n-p} \sum \left(\dfrac{q_{e,exp} - q_{e,cal}}{q_{e,exp}}\right)^2}$

with n is the number of the data points and p is the number of parameter within the model.

The adsorption of violet crystals into RB and RBA composites was found to fit the Langmuir better than the Freundlich equation thus suggesting that the adsorption has a homogeneous surface coverage; the *HYBRID* and *MPSD* error functions also resulting in lower values for Langmuir compared to Freundlich. A similar phenomenon also observed in the study by Oladipo et al., the chemisorption of crystal vio-

let onto A-AAB also found to be fitted well with Langmuir [25]. Brião et al. also found that the adsorption of crystal violet onto Chitin/ZSM-5 follows Langmuir better than the Freundlich equation [26].

Some comparison studies regarding the adsorption of crystal violet dye onto other adsorbents are summarized in Table 3. The use of rarasaponin to intercalate bentonite is
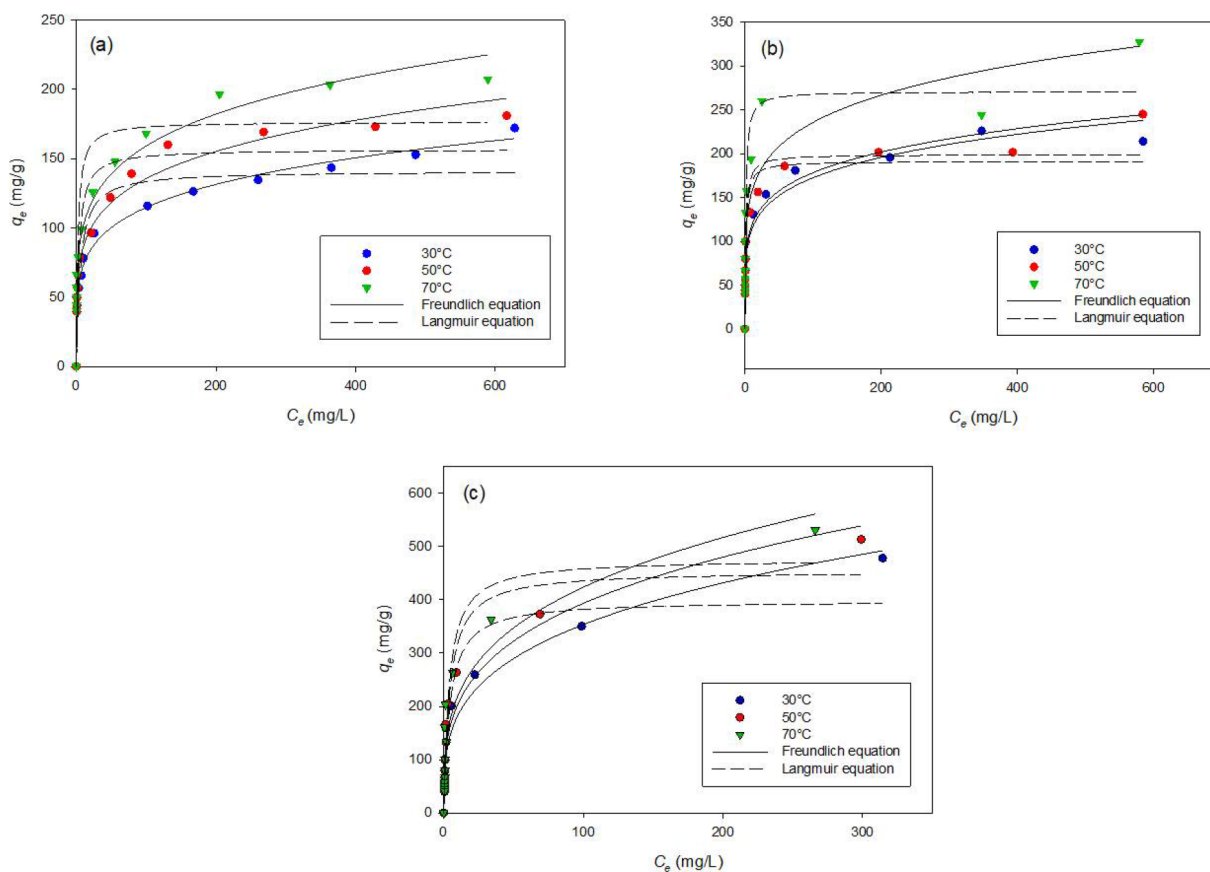

Fig. 8. Adsorption isotherms of crystal violet onto (a) AAB, (b) RB, and (c) RBA composite.

Table 3
Comparison study for the adsorption of crystal violet dye onto various adsorbent

Adsorbent[‡]	Characteristic	T (°C)	q_m (mg/g)	Isotherm model	Ref.
HDTMA-bentonite	Chemisorption	30	0.16 (365.11 µmol/g)	Freundlich	[27]
A-AAB	Chemisorption	25	582.4	Langmuir	[25]
Ch-GO/PUF	Chemisorption	35	64.935	Langmuir	[32]
Natural zeolite	Chemisorption	40	8.564	Freundlich	[28]
HDTMA-zeolite	Chemisorption	40	13.148	Freundlich	[28]
CTAB-zeolite	Chemisorption	40	5.539	Freundlich	[28]
Chitin/ZSM-5	Chemisorption	25	1217.3	Langmuir	[26]
AAB	Chemisorption	70	176.6300	Freundlich	This work
RB	Chemisorption	70	270.9195	Langmuir	This work
RBA composite	Chemisorption	70	476.0389	Langmuir	This work

[‡]Abbreviations: HDTMA, hexadecyltrimethylammonium; Ch-GO/PUF, chitosan-graphite oxide/polyurethane foam; CTAB, cetyltrimethylammonium bromide; Chitin/ZSM-5, Chitin/Zeolite Socony Mobil-5; A-AAB, alginate/ acid-activated bentonite; AAB, acid-activated bentonite; RB, rarasaponin-bentonite; RBA, rarasaponin-bentonite-alginate.

able to produce adsorbents with higher adsorption capacity than by using other surfactants; RB (in this study) can adsorb crystal violet dye up to 270.92 mg/g meanwhile HDTMA-bentonite only can adsorb 0.16 mg (365.11 µmol) crystal violet per g of adsorbent [27]. Karadag et al. showed that intercalation of HDTMA into another type of clay mineral, namely zeolite, also can increase the adsorption capacity but the intercalation of CTAB is failed to promote the adsorption capacity; where natural zeolite can adsorb 8.564 mg/g, HDTMA-zeolite 13.148 mg/g, and CTAB-zeolite 5.539 mg/g [28]. An excellent adsorption performance was shown by Chitin/ZSM-5 composite [26], from the study by Brião et al., where the Chitin/ZSM-5 composite can adsorb crystal violet dye 2.6 times (1217.3 mg/g) more than the RBA composite (476.04 mg/g) in this study. However, overall the adsorption performance of RBA composite is still comparable to the adsorbents listed in Table 3.

3.5. Adsorption kinetics studies

The adsorption kinetics experiments were conducted to understand the mechanism of the adsorption of crystal violet onto AAB, RB, and RBA composite. The pseudo-first-order and pseudo-second-order kinetic models were utilized to correlate the experimental data [29]. The mathematical expression for pseudo-first-order can be written as [30]:

$$q_e\left(1 - \exp(-k't)\right) = q_t \tag{6}$$

and the pseudo-second-order is expressed as [17]:

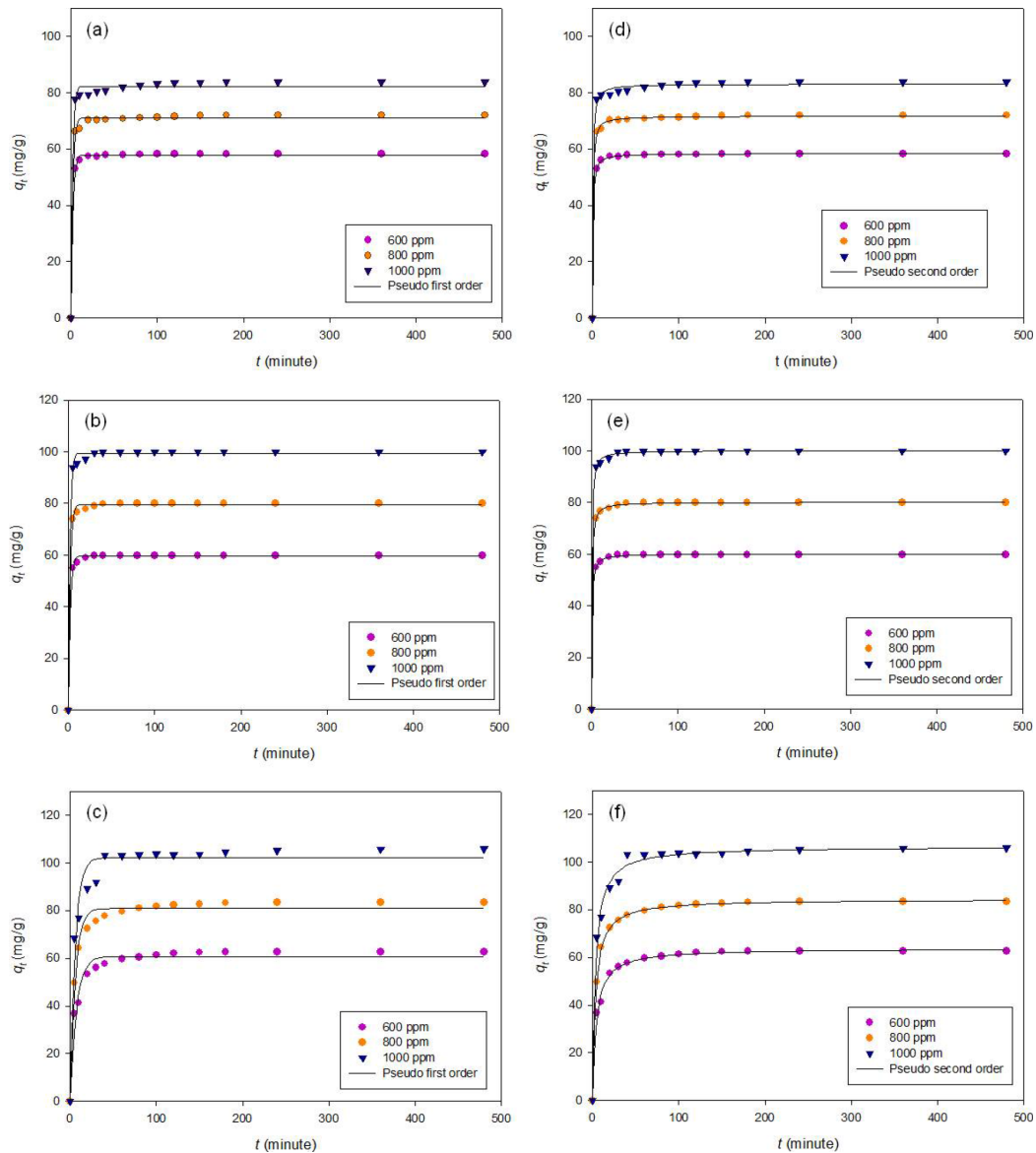$$q_t = \frac{k_s q_e^2 t}{\left(1 + \left(k_s q_e t\right)\right)} \tag{7}$$

Fig. 9. Adsorption kinetics of crystal violet onto (a, d) AAB, (b, e) RB, and (c, f) RBA composite.

Table 4
Pseudo-first and second order reaction kinetic parameters for the adsorption of crystal violet AAB, RB, and RBA composite

Initial crystal violet conc. (ppm)	$q_{e,exp}$ (mg/g)	Pseudo first order					Pseudo second order				
		k' (min⁻¹)	$q_{e,cal}$ (mg/g)	$R^{2\dagger}$	HYBRID§	MPSD‡	k_s (mg.g⁻¹.min⁻¹)	$q_{e,cal}$ (mg/g)	$R^{2\dagger}$	HYBRID§	MPSD‡
AAB											
600	58.1913	0.4831	57.8862	0.9990	0.4945	2.5595	0.0355	58.3945	0.9998	0.0804	1.0738
800	71.9238	0.5168	70.9664	0.9963	2.3267	4.9339	0.0291	71.6684	0.9993	0.6506	2.3726
1000	83.7341	0.5569	82.2333	0.9944	3.9674	7.1721	0.0273	83.0382	0.9978	2.3266	4.3457
RB											
600	59.9536	0.4942	59.6220	0.9984	0.6342	2.4268	0.0353	60.1485	0.9998	0.1804	1.4978
800	79.9042	0.5190	79.4548	0.9982	1.2597	3.5318	0.0287	80.1334	0.9998	0.1946	1.4459
1000	99.9066	0.5630	99.3535	0.9977	2.0002	3.6184	0.0267	100.1302	0.9996	0.3850	1.6471
RBA composite											
600	62.5557	0.1361	60.7381	0.9716	22.6320	19.6453	0.0037	63.7010	0.9953	4.0941	6.2156
800	83.3395	0.1681	80.8577	0.9832	14.3337	14.0250	0.0035	84.3589	0.9996	0.3977	2.0363
1000	105.7798	0.1711	102.1644	0.9650	28.7274	14.9088	0.0029	106.4786	0.9926	8.2470	8.1470

†R² is sum squares of residuals between calculated and experimental data; the value was obtained directly from data fitting by using Sigma plot.

§HYBRID $= \dfrac{100}{n-p} \sum \dfrac{\left(q_{t,exp} - q_{t,cal}\right)^2}{q_{t,exp}}$

‡MPSD $= 100 \sqrt{\dfrac{1}{n-p} \sum \left(\dfrac{q_{t,exp} - q_{t,cal}}{q_{t,exp}}\right)^2}$

with n is the number of the data points and p is the number of parameter within the model.

where q_e and q_t (mg/g) are the amounts of crystal violet adsorbed at equilibrium and at time t(min), respectively. Parameters k' (min⁻¹) and k_s (g mg⁻¹min⁻¹) are the time constant of pseudo-first-order and pseudo-second-order.

The adsorption kinetic plots and fitting by using the pseudo-first-order and pseudo-second-order models are depicted in Fig. 9, while the calculated parameters are summarized in Table 4. The kinetic studies were done at three different crystal violet dye concentrations. The value of parameter k' in the pseudo-first-order model increases with an increase in the initial concentration of crystal violet dye; this is because the time needed to reach the equilibrium condition is longer as the initial concentration increases so that the value of k' is smaller [17]. The parameter k' only able to show the rate of adsorption per minutes but cannot show the amount of crystal violet dye adsorbed per minutes. The pseudo-second-order model can give the correct prediction on the amount of crystal violet dye adsorbed per minutes from the parameter of time scaling factor k_s. As shown in Table 4, the value of k_s decreases with an increase in the initial concentration, which means that the amount of crystal violet dye adsorbed per minutes decreases with the increasing initial concentration of the dye.

The correlation between the empirical calculated data and the experimental data to pseudo-first-order and pseudo-second-order is found to be very good, this indicated by the R^2 values which are close to 1. As can be observed from the *HYBRID* and *MPSD* error function, the error values for the pseudo-second-order model are smaller than that of pseudo-first-order model; so that kinetics adsorption data was better fitted to the pseudo-second-order model than the pseudo-first-order model. The pseudo-first-order model was developed based on the assumption that mass transfer (physisorption) is more dominant in controlling the adsorption process, while the pseudo-second-order model assumes that chemical adsorption is the rate of determining step [31]. From the experiment of adsorption isotherm, it was found that chemisorption controls the adsorption mechanism; this is also supported by the result from the experiment of adsorption kinetics. In addition, the predicted value of q_e from the pseudo-second-order model is closer to that obtained experimentally (Table 4).

4. Conclusion

The new composite, namely RBA composite, has been successfully synthesized from bentonite, natural surfactant (rarasaponin), and natural polymer (sodium alginate). In the formation of RBA composite, the addition of rarasaponin induced intercalation process in the bentonite interlayer, while the addition of alginate as the natural polymer helps to join the particles of bentonite and rarasaponin. The addition of rarasaponin and alginate helps to increase the surface area of the adsorbent and increases the adsorption capacity. The RBA composite has the adsorption capacity two times higher than RB, and three times higher than the

AAB. The chemisorption was the dominant process that controlling the adsorption for all studied adsorbents.

Acknowledgment

References

[1] M. Neamtu, A. Yediler, I. Siminiceanu, M. Macoveanu, A. Kettrup, Decolorization of disperse red 354 azo dye in water by several oxidation processes - a comparative study, Dye. Pigment, 60 (2004) 61–68.

[2] P.K. Malik, S.K. Sanyal, Kinetics of decolourisation of azo dyes in wastewater by UV/H_2O_2 process, Sep. Purif. Technol., 36 (2004) 167–175.

[3] S. Chakraborty, M.K. Purkait, S.D. Gupta, S. De, J.K. Basu, Nanofiltration of textile plant effluent for color removal and reduction in COD, Sep. Purif. Technol., 31 (2003) 141–151.

[4] D. Chen, J. Chen, X. Luan, H. Ji, Z. Xia, Characterization of anion-cationic surfactants modified montmorillonite and its application for the removal of methyl orange, Chem. Eng. J., 171 (2011) 1150–1158.

[5] C.A.P. Almeida, N.A. Debacher, A.J. Downs, L. Cottet, C.A.D. Mello, Removal of methylene blue from colored effluents by adsorption on montmorillonite clay, J. Colloid Interface Sci., 332 (2009) 46–53.

[6] V.K. Gupta, R. Jain, A. Nayak, S. Agarwal, M. Shrivastava, Removal of the hazardous dye-Tartrazine by photo degradation on titanium dioxide surface, Mater. Sci. Eng. C., 31 (2011) 1062–1067.

[7] V.K. Gupta, A. Mittal, V. Gabje, J. Mittal, Removal and recovery of the hazardous azo dye acid orange 7 through adsorption over waste materials: Bottom ash and de-oiled soya, Ind. Eng. Chem. Res., 45 (2006) 1446–1453.

[8] M. Lezehari, J.P. Basly, M. Baudu, O. Bouras, Alginate encapsulated pillared clays: removal of a neutral/anionic biocide (pentachlorophenol) and a cationic dye (safranine) from aqueous solutions, Colloids Surfaces A Physicochem. Eng. Asp., 366 (2010) 88–94.

[9] A. Kurniawan, H. Sutiono, Y.H. Ju, F.E. Soetaredjo, A. Ayucitra, A. Yudha, S. Ismadji, Utilization of rarasaponin natural surfactant for organo-bentonite preparation: Application for methylene blue removal from aqueous effluent, Micropor. Mesopor. Mater., 142 (2011) 184–193.

[10] E. Fosso-Kankeu, F. Waanders, C.L. Fourie, Adsorption of Congo Red by surfactant-impregnated bentonite clay, Desal. Water Treat., 57 (2016) 27663–27671.

[11] A. Özcan, C. Ömeroğlu, Y. Erdoğan, A.S. Özcan, Modification of bentonite with a cationic surfactant: An adsorption study of textile dye Reactive Blue 19, J. Hazard. Mater., 140 (2007) 173–179.

[12] M.A. Zenasni, B. Meroufel, A. Merlin, B. George, Adsorption of Congo Red from aqueous solution using CTAB-kaolin from Bechar Algeria, J. Surf. Eng. Mater. Adv. Technol., 4 (2014) 332–341.

[13] H. Zaghouane-Boudiaf, M. Boutahala, Kinetic analysis of 2,4,5-trichlorophenol adsorption onto acid-activated montmorillonite from aqueous solution, Int. J. Miner. Process, 100 (2011) 72–78.

[14] A. Kurniawan, H. Sutiono, N. Indraswati, S. Ismadji, Removal of basic dyes in binary system by adsorption using rarasaponin–bentonite: Revisited of extended Langmuir model, Chem. Eng. J., 189–190 (2012) 264–274.

[15] O. Hamdaoui, Batch study of liquid-phase adsorption of methylene blue using cedar sawdust and crushed brick, J. Hazard. Mater., 135 (2006) 264–273.

[16] K.V. Kumar, K. Porkodi, F. Rocha, Comparison of various error functions in redicting the optimum isotherm by linear and non-linear regression analysis for the sorption of basic red 9 by activated carbon, J. Hazard. Mater., 150 (2008) 158–165.

[17] B. Subramanyam, A. Das, Linearised and non-linearised isotherm models optimization analysis by error functions and statistical means, J. Environ. Health Sci. Eng., 12 (2014) 92.

[18] K.V. Kumar, Linear and non-linear regression analysis for the sorption kinetics of methylene blue onto activated carbon, J. Hazard. Mater., 137 (2006) 1538–1544.

[19] J. Sreńscek-Nazzal, U. Narkiewicz, A.W. Morawski, R.J. Wróbel, B. Michalkiewicz, Comparison of optimized isotherm models and error functions for carbon dioxide adsorption on activated carbon, J. Chem. Eng. Data, 60 (2015) 3146–3158.

[20] M. Doğan, M. Alkan, Ö. Demirbaş, Y. Özdemir, C. Özmetin, Adsorption kinetics of maxilon blue GRL onto sepiolite from aqueous solutions, Chem. Eng. J., 124 (2006) 89–101.

[21] K.Y. Lee, D.J. Mooney, Alginate: properties and biomedical applications, Prog. Polym. Sci., 37 (2012) 106–126.

[22] A.S. Waldman, L. Schechinger, G. Govindarajoo, J.S. Nowick, L.H. Pignolet, The alginate demonstration: polymers, food science, and ion exchange, J. Chem. Educ., 75 (1998) 1430–1431.

[23] E. Nathaniel, A. Kurniawan, F.E. Soetaredjo, S. Ismadji, Organo-bentonite for the adsorption of Pb(II) from aqueous solution: Temperature dependent parameters of several adsorption equations, Desal. Water Treat., 36 (2011) 280–288.

[24] I. Langmuir, The constitution and fundamental properties of solids and liquids. Part I. Solids, J. Am. Chem. Soc., 38 (1916) 2221–2295.

[25] A.A. Oladipo, M. Gazi, Enhanced removal of crystal violet by low cost alginate/acid activated bentonite composite beads: Optimization and modelling using non-linear regression technique, J. Water Process Eng., 2 (2014) 43–52.

[26] G.V. Brião, S.L. Jahn, E.L. Foletto, G.L. Dotto, Adsorption of crystal violet dye onto a mesoporous ZSM-5 zeolite synthetized using chitin as template, J. Colloid Interface Sci., 508 (2017) 313–322.

[27] T.S. Anirudhan, M. Ramachandran, Adsorptive removal of basic dyes from aqueous solutions by surfactant modified bentonite clay (organoclay): Kinetic and competitive adsorption isotherm, Process Saf. Environ., 95 (2015) 215–225.

[28] D. Karadag, E. Akgul, S. Tok, F. Erturk, M.A. Kaya, M. Turan, Basic and reactive dye removal using natural and modified zeolites, J. Chem. Eng. Data, 52 (2007) 2436–2441.

[29] S. Lagergren, About the theory so-called adsorption of soluble substances, K. Sven. Vetenskapsakad Handl., 24 (1898) 1–39.

[30] N. Belhouchat, H. Zaghouane-Boudiaf, C. Viseras, Removal of anionic and cationic dyes from aqueous solution with activated organo-bentonite/sodium alginate encapsulated beads, Appl. Clay. Sci., 135 (2017) 9–15.

[31] W. Plazinski, W. Rudzinski, A. Plazinska, Theoretical models of sorption kinetics including a surface reaction mechanism: A review, Adv. Colloid Interface Sci., 152 (2009) 2–13.

[32] J. Qin, F. Qiu, X. Rong, J. Yan, H. Zhao, D. Yang, Adsorption behavior of crystal violet from aqueous solutions with chitosan-graphite oxide modified polyurethane as an adsorbent, J. Appl. Polym. Sci., 132 (2015) 41828 (10 pages).